Phys. Status Solidi A **209**, No. 10, 1884–1893 (2012) / **DOI** 10.1002/pssa.201200216

Part of Topical Section on
Advanced Silicon Materials for Electronics and Photovoltaics

physica status solidi a
www.pss-a.com
applications and materials science

Feature Article

Recombination via point defects and their complexes in solar silicon

A. R. Peaker[*,1], **V. P. Markevich**[1], **B. Hamilton**[1], **G. Parada**[2], **A. Dudas**[2], **A. Pap**[2], **E. Don**[3], **B. Lim**[4], **J. Schmidt**[4], **L. Yu**[5], **Y. Yoon**[5], **and G. Rozgonyi**[5]

[1] Photon Science Institute, University of Manchester, Manchester M13 9PL, UK
[2] Semilab, 2 Prielle Kornelia Str, 1117 Budapest, Hungary
[3] Semimetrics, PO Box 36, Kings Langley, Herts WD4 9WB, UK
[4] Institute for Solar Energy Research (ISFH) Hamlen, 31860 Emmerthal, Germany
[5] Department of Materials Science and Engineering, North Carolina State University, Raleigh, NC 27695-7907, USA

Received 30 May 2012, revised 6 September 2012, accepted 7 September 2012
Published online 6 October 2012

Keywords Laplace deep level transient spectroscopy, minority carrier lifetime, passivation, recombination, silicon solar cells, transition metals

* Corresponding author: e-mail a.peaker@manchester.ac.uk, Phone: +44 161 306 4752

Electronic grade Czochralski and float zone silicon in the as grown state have a very low concentration of recombination generation centers (typically $<10^{10}\,cm^{-3}$). Consequently, in integrated circuit technologies using such material, electrically active inadvertent impurities and structural defects are rarely detectable. The quest for cheap photovoltaic cells has led to the use of less pure silicon, multi-crystalline material, and low cost processing for solar applications. Cells made in this way have significant extrinsic recombination mechanisms. In this paper we review recombination involving defects and impurities in single crystal and in multi-crystalline solar silicon. Our main techniques for this work are recombination lifetime mapping measurements using microwave detected photoconductivity decay and variants of deep level transient spectroscopy (DLTS). In particular, we use Laplace DLTS to distinguish between isolated point defects, small precipitate complexes and decorated extended defects. We compare the behavior of some common metallic contaminants in solar silicon in relation to their effect on carrier lifetime and cell efficiency. Finally, we consider the role of hydrogen passivation in relation to transition metal contaminants, grain boundaries and dislocations. We conclude that recombination via point defects can be significant but in most multi-crystalline material the dominant recombination path is via decorated dislocation clusters within grains with little contribution to the overall recombination from grain boundaries.

© 2012 WILEY-VCH Verlag GmbH & Co. KGaA, Weinheim

1 Introduction The last decade has witnessed a commercial and technological revolution in silicon photovoltaics. The quest for viable renewable energy sources has resulted in many countries establishing policies, which provide taxation advantages or feed in tariffs to encourage the take up of renewable energy. This has been remarkably successful and has had the desired effect of stimulating the market enabling successful manufacturers to effect reductions in manufacturing cost. Silicon photovoltaics have benefited from this and progress along the learning curve necessary to achieve economies of scale in manufacture has been very rapid (a learning rate of 20% compared to an industry norm of 10%, i.e. a cost reduction of PV systems by 20% for each doubling of cumulated PV installations).

There are many factors involved in this but innovative cell design, the use of low cost materials and advances in power management electronics have each played a role. In particular, the cost of silicon in the cell, which used to be ~50% of the cell value, has been reduced by using thinner slices and moving away from electronic grade single crystal material grown as Czochralski (Cz) ingots to less pure "solar grade" silicon usually cast in multicrystalline blocks. Although such material produces cells of lower conversion efficiency than electronic grade silicon, a cost reduction per kWh delivered is achieved because the reduction in efficiency is more than compensated for by the lower price of the silicon. Market research (e.g. Solarbuzz) shows that >85% of new installations use

© 2012 WILEY-VCH Verlag GmbH & Co. KGaA, Weinheim

wafered silicon cells of multi crystalline or single crystal material.

The term "solar grade silicon" does not have a unique definition. It has been used to describe Cz silicon grown from silicon scrap feedstock, block cast multi-crystalline material with electronic grade feedstock or silicon grown from feedstock that has been produced by a refining process less energy hungry (and less effective) than the electronic grade Siemens process. These include fluidized bed methods and in the extreme improved metallurgical (IMG) silicon. These materials contain higher concentrations of metals than electronic grade material and in some cases higher carbon content. This can originate from upgraded metallurgical extraction methods or from casting highly refined silicon in graphite crucibles. Such material can contain concentrations of carbon in solution around the equilibrium solubility at the melting point ($3.5 \times 10^{17}\,cm^{-3}$) and SiC particles.

In cast, multi-crystalline silicon the presence of grain boundaries and dislocations makes the material inhomogeneous in terms of its electronic properties. An example of this inhomogeneity can be seen in Fig. 1 which shows a variation of 25% in lifetime. Comparison with a map of the grains in this slice shows that the excess recombination is not associated with the grain boundaries but rather with regions within specific grains, which we associate with decorated dislocation clusters. A lifetime map of present day state of the art electronic grade single crystal material (Cz or FZ) shows a variation of minority carrier lifetime of $\sim$1% with edge exclusion.

The combination of the structural defects, metal content and precipitates of various sizes make defect reactions extremely complex and the material very difficult to assess by conventional techniques. The pragmatic approach of the solar industry is to measure average properties assigning a single lifetime to the whole slice ($\sim$5 inch square). In many cases, this works quite well at least in terms of deciding if material is worth processing into cells but such averaging is not adequate in trying to understand the localized recombination paths and improving the material.

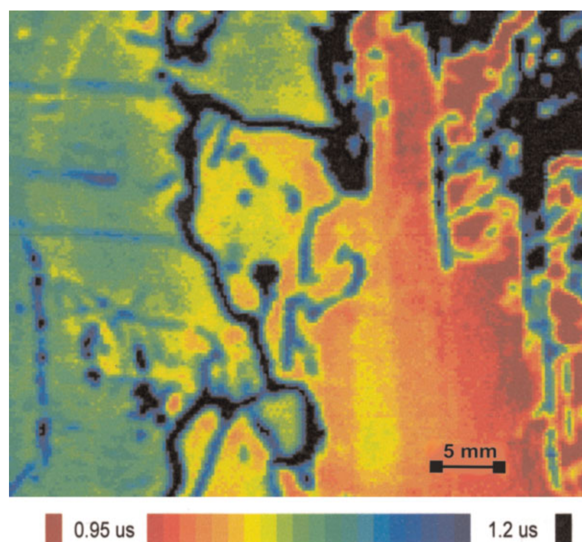

Figure 1 (online color at: www.pss-a.com) Map of the minority carrier lifetime of a silicon nitride passivated multi-crystalline silicon slice taken from near the top of a cast ingot. The low lifetime is due to high concentrations of metallic impurities and dislocations. The map was taken using a Semilab WT-2000 PVN in the μPCD mode with a 0.5 mm diameter 904 nm laser probe and a background illumination of one sun.

Originally, it was thought that grain boundaries acted as important recombination centers in mc-Si but it now seems that this is not often the case. In recent material, the grains are very much larger than the diffusion length in equivalent single crystal material. In addition, the grain boundaries are mostly parallel to the direction of carrier flow in the cell. These factors result in recombination at grain boundaries being a relatively small perturbation in terms of cell efficiency or minority carrier lifetime whereas decorated dislocations and dislocation clusters are much more significant as will be discussed later.

In this paper, we consider solar silicon in two stages. Firstly, we review single crystal materials containing metals including some of our recent measurements, which try to resolve discrepancies and which consider small precipitates and their passivation with hydrogen.

In general, transition metals particularly those in the 3d series, are common contaminates in lower grade feedstock. These will act as recombination centers if present in the finished solar cell on specific sites. This provides some insight into Cz material grown from impure feedstock as a solar cell material. We then consider multi-crystalline solar silicon with similar contamination and explore the role of grain boundaries, dislocations and precipitates in the minority carrier recombination processes.

This necessitates localized measurements of specific grains and grain boundary regions. In combination with hydrogen passivation this provides us with a basis for understanding some of the efficiency limitations, which occur in this very complex material system.

2 Metallic contamination in single crystals

2.1 Impact on cell efficiency: An overview

There is a vast literature on metals in silicon with an emphasis on the transition metals, some of these publications focus on photovoltaics. An early experiment, known as the Westinghouse study [1] added contaminants to a Czochralski melt and pulled small ingots of both n and p-type material (3.3 cm diameter grown at $7\,cm\,h^{-1}$). Chemical concentrations of impurities in slices cut from the ingots were measured using neutron activation analysis and spark source mass spectrometry.

Concentrations of electrically active defects were measured in some slices using deep level transient spectroscopy (DLTS). Solar cells were fabricated (both n^+p and p^+n) with and without an antireflection layer and the efficiency measured. In all approximately 200 ingots were grown and processed into solar cells. Although there was no

© 2012 WILEY-VCH Verlag GmbH & Co. KGaA, Weinheim

intentional hydrogen passivation the contacts were sintered at 300–550 °C in hydrogen.

The efficiency of uncontaminated cells was found to be around 10% with no antireflection layer and 14% with a silicon dioxide antireflection film.

The impact of various impurities is shown in Fig. 2 in terms of the effect of chemical concentration of metals in the slices cut from the various ingots on the solar cell efficiency for the case of a p-type base. It is important to emphasize that these results convolute many factors apart from the Shockley–Read–Hall (SRH) properties of the defect state associated with the metal. Not all the metal will be electrically active in the slice, the n^+ layer diffusion will tend to getter metals with high diffusivity and growth of precipitates may occur during cell processing.

DLTS measurements for some of the metals have been published as part of the Westinghouse study and the concentration of specific gap states compared with the chemical concentrations. These are tabulated elsewhere [1] as values of the ratio N_T/N_{chem}. These are specific to the elements concerned but for Cr, V, Ti, and Mo are independent of the concentration over the range studied (up to 10^{14} cm^{-3}) suggesting that precipitation did not occur during ingot cooling for these elements under the conditions used. For example, all of the Mo was present as an electrically active species at $E_v + 0.3$ eV, Ti had a ratio of 0.4 for a defect at $E_v + 0.3$ eV, the Cr ratio was 0.23 for a state at $E_v + 0.22$ eV. Cu and Ni were exceptional in that no electrically active defects could be detected. In the light of what we know today this is not unexpected. In the case of Cu its extremely high diffusivity in p-type would remove it to energetically preferred sites (surface and precipitates) where it might be electrically inactive as a recombination center. It must however be emphasized that some precipitates can act as recombination centers and can also degrade solar cells by acting as current leakage paths (shunts) which affect the IV characteristic of solar cell and reduce its efficiency by the effect on the fill factor.

The phenomena of precipitation will be discussed in more detail later but at this stage we can say that in the Westinghouse experiment over the range of metal concentrations studied the recombination activity impairing the solar cell efficiency associated with the added impurities was due to metals in solution, i.e. the classic point defects which are well characterized in terms of their recombination behavior.

In uncontaminated, as grown, electronic grade Cz material the concentration of electrically active defects behaving as recombination centers is vanishingly small. This is a result of high purity feedstock and the low segregation coefficient, k_{eff}, between the solid and the melt in Cz growth. For most of the 3d transition metals, k_{eff} lies between 10^{-8} and 10^{-5} (k_{eff} = impurity concentration in ingot/impurity concentration in melt). This is a great advantage to those companies growing Cz Si from lower purity cost feedstocks.

In our work on single crystal silicon, we have also used some material in which metals have been incorporated during Cz and FZ growth but the studies we report here have mostly been done on electronic grade Cz or FZ material into which specific metals have been introduced by diffusion.

2.2 Solubility and diffusivity The solubility and diffusivity of contaminant metals are central to understanding their effects in solar silicon. For the 3d transition metals diffusion is almost exclusively interstitial over a wide temperature range but there is a systematic increase in both solubility and diffusivity in the 3d series progressing from the light to the heavy elements as can be seen in Fig. 3.

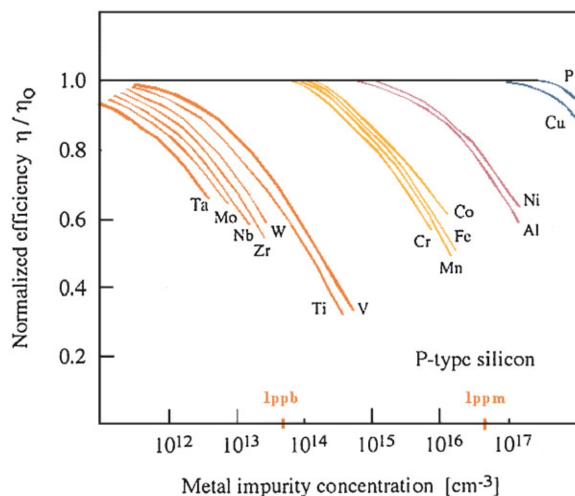

Figure 2 (online color at: www.pss-a.com) The effect of metallic contaminants on solar cell efficiency. The impurity concentration is that in the slice prior to cell processing. The data are taken from the Westinghouse experiment [1] and re-plotted by Pizzini et al. [2].

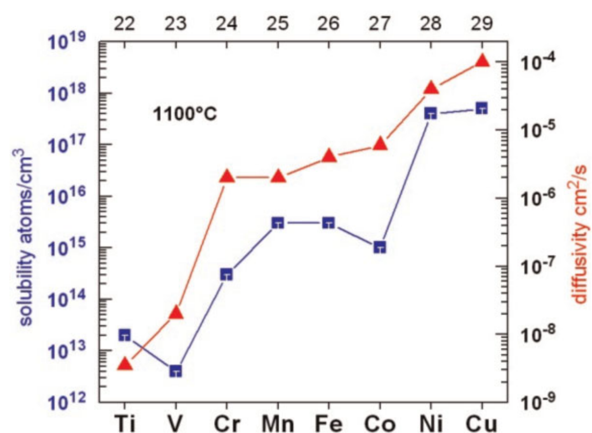

Figure 3 (online color at: www.pss-a.com) Solubility (squares) and diffusivity (triangles) of 3d transition metals plotted in the sequence of their atomic number. These physical properties are the primary cause of the sequencing of the 3d metals in Fig. 2.

© 2012 WILEY-VCH Verlag GmbH & Co. KGaA, Weinheim

Table 1 Solubility and diffusivity in silicon.

species	solubility* (atoms cm^{-3})	diffusivity* ($cm^2 s^{-1}$)	notes and references
Ti	2×10^{13}	3.5×10^{-9}	Ti_i DLTS [5]
V	4×10^{12}	2×10^{-8}	V_i DLTS [6]
Cr	3×10^{14}	2×10^{-6}	NAA see Ref. [7]
Mn	3×10^{15}	2×10^{-6}	NAA see Ref. [7]
Fe	3×10^{15}	4×10^{-6}	NAA [8], tracer [9]
Co	10^{15}	6×10^{-6}	tracer [10]
Ni	4×10^{17}	4×10^{-5}	NAA [11]
Cu	5×10^{17}	1×10^{-4}	tracer [9, 12]
Mo (4d)	$\sim 10^{14}$	9×10^{-10}	DLTS [13]
Au (5d)	10^{16}	8×10^{-8}	tracer [9]
B	2×10^{20}	1×10^{-13}	
P	10^{21}	3×10^{-13}	

*At 1100 °C.

A combination of high concentration and high diffusivity will result in precipitation on cooling either at surfaces and interfaces or at nucleation centers such as dislocations. Copper is the classic example precipitating as lamina usually lying in {111} planes [3] and often referred to as copper colonies.

Copper has a high diffusivity in p-type material even at room temperature and so is unstable in its interstitial form. A consequence of this is that only a small fraction of copper in silicon is electrically active ($\sim 10^{-4}$) as complexes or as Cu_s [3]. The remainder is present as dislocation decoration or large precipitates (which have few electrically active states compared to the number of copper atoms). The presence of such precipitates can be very detrimental to the finished cell by acting as a shunt across the junction.

At the other extreme of the 3d metals, titanium has a very low solubility and diffusivity. This results in very small or no precipitates [4] and a large part (0.4) of the Ti being electrically active on interstitial sites. It is these phenomena, which explain the results of the Westinghouse experiment shown in Fig. 2 rather than a difference in the recombination properties of the species in solid solution.

Table 1 lists solubility and diffusivity data at 1100 °C for the 3d transition metals and for Mo and Au. B and P data are included for comparison. Where available the results of chemical methods are cited in preference to electrical techniques, which may only be valid for one configuration or charge state of the species.

2.3 Recombination kinetics Recombination via point defects is usually described by SRH kinetics in which the recombination rate is proportional to the defect concentration and a property of the defect quantified as the minority carrier capture cross section. The dominant factor determining the cross section is the charge state of the defect so that a donor (positively charged) will repel holes but attract electrons. In the case of low level excitation and a near mid gap state in silicon at room temperature these are the only parameters of importance so the lifetime due to SRH via point defects can be expressed for p-type material as

$$\tau_n = \frac{1}{N_T \sigma_n V_{th}}, \tag{1}$$

where V_{th} is the thermal velocity, N_T the defect concentration and σ_n the minority carrier capture cross section.

However, solar cells do not always operate in a low excitation regime. At an intensity of one sun the excess carrier population is below the usual doping level of the base but sufficiently high to necessitate taking into account the possible saturation of some defects. Saturation starts to occur when the majority carrier capture rate is comparable with the minority carrier capture rate. This effect is easily observed in lifetime measurements as shown in Fig. 4 which shows lifetime dependencies resulting from different concentrations of boron–oxygen recombination center.

The saturation behavior depends on the ratio of the minority and majority cross-sections, on the doping level of the sample and the temperature. It follows that such measurements can be used to determine σ_n/σ_p if a single species is dominant. The cases of boron–oxygen [14] and for chromium and cobalt [15] are referred to as examples. The σ_n/σ_p parameter may be an aid to identifying the defect species responsible for the lifetime degradation. Such "identification" is only feasible if the cross section ratios of the potential contaminants are known. In some samples, surface recombination and trapping in passivating layers can complicate the interpretation of lifetime dependency on excitation density.

The second case where Eq. (1) is too simplistic is where the state is sufficiently near one of the bands energetically for the thermal emission rate to be a significant fraction of capture rate. This thermalization reduces the recombination

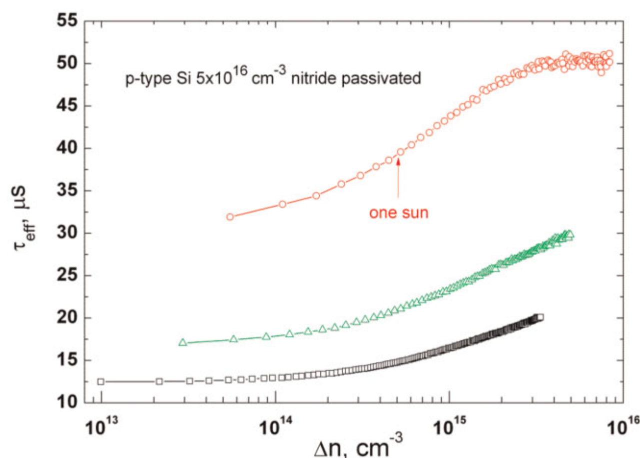

Figure 4 (online color at: www.pss-a.com) Effect of excitation density on minority carrier lifetime. These data were recorded using a Semilab WT-2000 PVN in which the lifetime is measured using the μ-PCD technique. A 903 nm LASER is used to create the small carrier perturbation whose decay is measured. A second LASER creates the background excitation density in this case up to 14 suns.

 © 2012 WILEY-VCH Verlag GmbH & Co. KGaA, Weinheim

rate and again it can be used as a tool to determine the parameters of the recombination center [16].

Both these processes are quantified in the detailed SRH formalism, which is presented in many standard texts [17] as well as in the original papers. In summary, in p-type material a positively charged defect (donor or double donor) will exhibit a large capture cross section for electrons (minority carriers) and hence could be an important recombination center. However, in order to continue to capture minority carriers it must also capture majority carriers. If the defect is doubly positively charged (i.e. a double donor) then the capture of the electrons will be very fast but majority carrier capture will be slow and saturation will be observed at low excitation densities unless the material is heavily doped. In the case of a single donor minority carrier capture will be quite fast but majority carrier capture will be into a neutral center, again saturation will be observed but at a higher excitation density than for the double donor case.

Table 2 lists some of the published data on the energy levels of transition metals in silicon. It must be emphasized that this is a selection from a vast amount of data in the literature. Where a review exists comparing differing results this is cited. Specifically excluded are those data inferring capture cross-sections from DLTS emission data using detailed balance. Such data can give values, which exceed the directly determined values by several orders of magnitude.

Table 2 Electrically active states associated with transition metals in silicon.

species	energy (meV)	cross sections* (cm^2)	notes and references
$Ti_i^{+/++0}$	$E_v + 255$	$\sigma_p^* = 3.8 \times 10^{-17}$	DLTS [18]
		$\sigma_n^* = 1.3 \times 10^{-14}$	
$Ti^{0/+}$	$E_c - 271$	$\sigma_p = 1.35 \times 10^{-15}$	
$Ti^{-/0}$	$E_c - 90$	$\sigma_n^* = 3 \times 10^{-14}$	
$V_i^{+/++}$	$E_v + 340$	$\sigma_p^* = 1.2 \times 10^{-16}$	DLTS [19]
$V_i^{0/+}$	$E_c - 450$	$\sigma_n = 5.3 \times 10^{-15}$	
$V_i^{-/0}$	$E_c - 200$	$\sigma_n = 1.2 \times 10^{-16}$	
$Cr^{0/+}$	$E_c - 230$		DLTS [20]
$(CrB)^{0/+}$	$E_v + 280$		
$Mn^{+/++}$	$E_v + 250$		DLTS
$Mn^{0/+}$	$E_c - 420$		see Ref. [21]
$Mn^{-/0}$	$E_c - 110$		
$Fe_i^{0/+}$	$E_v + 385$	$\sigma_p^* = 8 \times 10^{-17}$	DLTS/Hall
		$\sigma_n = 4 \times 10^{-14}$	see Refs. [6, 22]
$(FeB)^{0/+}$	$E_v + 100$	$\sigma_p = 3 \times 10^{-15}$	
$(FeB)^{-/0}$	$E_c - 260$	$\sigma_n = 10^{-15}$	
Co			see Ref. [3]
Ni			see Refs. [11, 3]
Cu			see Ref. [3]
Mo (4d)	$E_v + 300$	$\sigma_p = 5.5 \times 10^{-16}$	DLTS [13]
$Au^{0/+}$ (5d)	$E_v + 350$	$\sigma_n = 1.1 \times 10^{-15}$	MCTS [23]
		$\sigma_p^* = 1 \times 10^{-15}$	MCTS [23]
$Au^{-/0}$	$E_c - 558$	$\sigma_n = 8.7 \times 10^{-17}$	DLTS [23]
		$\sigma_p^* = 8 \times 10^{-15}$	DLTS [23]
$(AuH)^{-/0}$	$E_c - 542$	$\sigma_n = 6 \times 10^{-17}$	LDLTS [24]
$(AuH)^{-/-}$	$E_c - 193$		DLTS [25]
$(AuH_2)^{-/0}$	$E_c - 578$		LDLTS [25]

*Significant dependence of the capture cross section on temperature, see references.

Some of the transition metals form complexes with acceptors. In p-type material, the best-known case is that of FeB. The interstitial iron is positively charged and is coulombically attracted to the negatively charged boron acceptor. The result is that FeB pairs are the room temperature equilibrium state but are dissociated in the presence of minority carriers. This dissociation is used as a test for iron because although both Fe_i and FeB are important recombination centers Fe_i has more impact on the lifetime than FeB at low excitation densities consequently a measure of the change of lifetime on dissociation of the FeB pair has become a standard test for iron contamination in Si within the PV industry. However, care must be exercised as at high excitation densities the FeB pair is a more effective recombination center and so the excitation density affects the [Fe] lifetime relationship and hence the calibration [26, 27]. In machines such as the Semilab WT-2000 PV an iron test procedure is built into the operating system so ensuring that the correct test conditions are always used.

The FeB pair is well understood as a complex in silicon but as we progress along the 3d series in the periodic table to the heavier elements with the highest diffusivities the situation becomes much more difficult to predict. In particular, Co, Ni, and Cu diffuse interstitially but are more likely to form complexes rather than stable interstitial recombination centers or to form a simple pair with an acceptor as is the case with the lighter 3d elements. We discuss this behavior in Section 2.5.

2.4 Passivation with hydrogen A crucial part of solar cell fabrication is the use of anti-reflection films, which also incorporate hydrogen. The classic case is silicon nitride deposited by plasma assisted chemical vapor deposition (plasma CVD). Such films contain high concentrations of hydrogen. The exact amount depends on the deposition conditions but 25 at% hydrogen is fairly typical for films used in silicon solar cells. Silicon nitride acts as a source of hydrogen during subsequent processing. This dramatically reduces surface recombination but also some hydrogen diffuses into the bulk of the silicon and passivates recombination centers. The details of this process are the subject of debate but what is certain is that the incorporation of hydrogen into solar silicon increases the minority carrier lifetime considerably.

In silicon, hydrogen diffuses predominantly interstitially in atomic form. It exists as H^+ at a bond center site in p-type material and H^- at an interstitial tetrahedral site in n-type, the neutral state H^0 being metastable. The donor level lies above the acceptor level, with the consequence that monatomic hydrogen behaves as a negative-U defect in silicon. The behavior is reviewed in detail elsewhere [28].

© 2012 WILEY-VCH Verlag GmbH & Co. KGaA, Weinheim

Both the positive and negative ions are very reactive so as the hydrogen ions migrate through the lattice they combine with the unsatisfied bonds of defects and impurities rendering them electrically inactive or in some cases shifting the electronic levels within the gap. The most obvious reaction is with the shallow donors and acceptors forming pairs, which are electrically inactive. However the binding is quite weak (e.g. BH 1.28 eV and PH 1.2 eV). The BH bond is dissociated at low annealing temperatures ($\sim$200 °C) freeing the hydrogen to continue its migration and enabling it to passivate recombination centers. The PH pair is also dissociated in the presence of holes.

In the case of the transition metals, many hydrogen reactions have been reported. In general there is the possibility of binding with several hydrogen ions to form (TM)H_n The addition of hydrogen shifts the TM energy level in the gap and may render it electrically inactive (passivated).

Only in a relatively few cases is the sequence of reactions clearly documented. In the case of platinum all the three complexes PtH_n ($n=1$–3) have been unambiguously identified by a combination of DLTS, EPR, and LVM [see 28 for a compilation of references]. In the case of AuH and AuH_2 the addition of hydrogen shifts the level in the gap. Figure 5 illustrates the small shift observed which is barely detectable in conventional DLTS but can be seen clearly with the Laplace DLTS technique [29]. Annealing at 250 °C removes the hydrogen from the gold resulting in a reduction of the G4 peak and an increase in the Au peak [24]. The reaction is reversible in the presence of free hydrogen. AuH_2 has been seen in the same way [25].

The situation with the predominantly interstitial TMs may follow a similar pattern but seems to be more complex. Many electrically active states have been reported as a result of hydrogenation (see Ref. [30] for citations) but there is a worrying lack of consistency. In some cases passivation has been inferred from a reduction in the total number of electrically active states, i.e. the electrically active [TM] prior to passivation is greater than the electrically active [TM]H_n after passivation. In general reactions with H^+, in p-type Si with the TM interstitial ion in a positively charged state seems highly improbable unless minority carriers are present, e.g. $Ti_i^+ + e \rightarrow Ti_i^0$ which can then react with H^+ or H^0 [31]. That paper and first-principle studies of hydrogen reactions [32] illustrate very clearly that these are difficult systems to understand in detail.

The situation is even more complex for the heavier 3d metals, which diffuse faster and tend to form larger complexes. Although electrically active states have been observed after hydrogenation of Ni or Cu doped Si [33, 34], theoretical studies are not consistent with Ni_iH_n or Cu_iH_n but may be related to substitutional fractions of Ni or Cu [32, 35, 36]. The emphasis is on the word ‘‘may’’ because at least eleven distinctly different DLTS lines have been reported for nickel hydrogen complexes and many more for the copper hydrogen case.

This leaves us in a very unsatisfactory position because we observe experimentally a substantial improvement in lifetime in mc-Si after hydrogenation but do not understand explicitly what is being passivated (apart from the surface) and more importantly what is not being passivated. Increasing the carrier lifetime in solar silicon is crucial if major improvements in efficiency are to be achieved. Gettering plays a key role in removing the fast diffusing species from the active region of the cell but is less effective for the slower diffusing elements or for fast diffusants trapped in relatively stable configurations. These can be powerful recombination centers where probably the only route to removing them is by passivation.

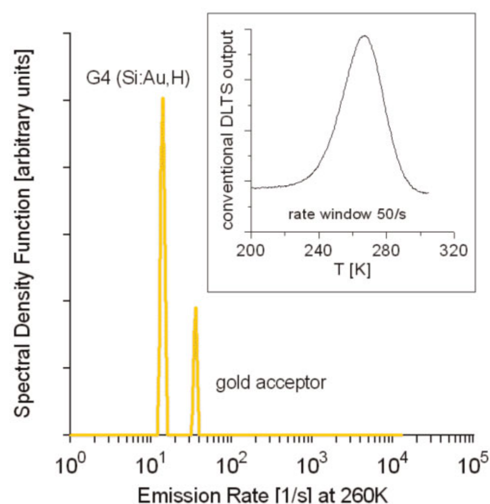

Figure 5 (online color at: www.pss-a.com) Comparison of Laplace DLTS and conventional DLTS measurements of electron emission form a silicon sample doped with gold and hydrogen [24]. Laplace DLTS clearly distinguishes the gold hydrogen from the gold emission characteristics.

3 Defect complexes and dislocations One of the reasons for the problems in understanding the behavior of the heavier 3d transition metals is that their high diffusivity facilitates the formation of complexes. The highly mobile interstitial migrates through the lattice until it finds an energetically favorable site. This can be bonding with another impurity (the FeB defect already discussed is a classic case), with an intrinsic defect or with itself. These complexes can consist of just two atoms or large precipitates, which strain the lattice and act as favorable sites for more mobile impurities. It is often the case on analyzing such defects that more than one element is present so, for example, the strain field in the vicinity of a copper silicide particle could trap nickel or iron.

In general, it seems that such accumulations of metals are not very recombination active but can be important in creating leakage paths. Micro-Raman techniques are immensely valuable in mapping the strain field around such precipitates and other extended defects [37]. Early impressions are that much can be learned by comparing lifetime maps with localized strain measurements.

 © 2012 WILEY-VCH Verlag GmbH & Co. KGaA, Weinheim

3.1 Dislocations and decoration The strain field of a dislocation can be a sink for fast diffusing species. This is important because there is now overwhelming evidence that absolutely clean dislocations are not important recombination centers and have little electrical activity but decorated dislocations can degrade lifetime. Early measurements of electrical activity were undertaken on plastically deformed silicon [38]. It now seems that these samples were contaminated with metals from the bending jig and so these early results described decorated dislocations.

Subsequent measurements on the Frank partial dislocations surrounding stacking faults (which could be created in ultra clean conditions) showed that the electrical properties and recombination activity depended very strongly on the level of decoration. This is the case in both n-type [39] and p-type [40]. The electrically active defects, determined by DLTS, were found to increase in concentration and move deeper in the gap with an increasing concentration of metal concentration, so increasing the recombination activity, until micro-precipitates started to be observed on the dislocation by TEM. At this point the electrical activity diminished rapidly [41].

The concept of dislocation decoration has been embedded into a model describing the observed EBIC contrast [42]. More recently enhancement of recombination behavior by decoration at grain boundaries has been explored using a model system based on mis-orientated bonded wafers [43]. These observations are of crucial importance in mc-Si which contains grain boundaries, dislocations and an ample supply of TM impurities to effect decoration.

3.2 Small complexes In addition to these defects, which consume considerable numbers of metal atoms there is evidence of small complexes consisting of between three and ten atoms.

Historically, photoluminescence (PL) has been very effective in identifying such defects. Recently, the topic has advanced rather spectacularly by the use of isotopically pure silicon and the implantation of radioactive isotopes using the ISOLDE facility at CERN. This and earlier work on PL of TMs in silicon has been the subject of an Applied Physics Review [44].

Importantly, a number of four and five atom families have been revealed including Cu complexes some of which have been the subject of *ab initio* calculations [45].

DLTS peaks associated with extended defects such as decorated dislocations and silicide precipitates are broad with a carrier capture which slows as more carriers are accumulated because the extended defect becomes coulombically repulsive. This is sometimes referred to as logarithmic filling.

In Laplace DLTS, the instrumental broadening characteristic of the conventional technique has been eliminated so a perfect point defect gives a delta like function on the emission rate scale. The peaks shown in Fig. 5 are typical of ideal isolated point defects. Broadening can occur due to field dependence of the emission or to inhomogeneous strain. However, Laplace DLTS confers little benefit to the study of extended defects where the broadening is a fundamental physical process and very substantial.

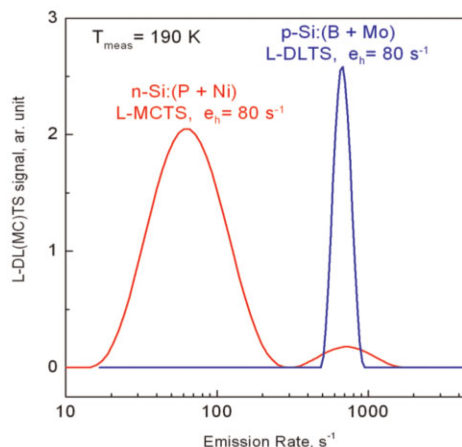

Figure 6 (online color at: www.pss-a.com) Laplace DLTS of two hole traps observed in silicon. The peak at the right is due to Mo in p-type Si while the peak on the left is associated with Ni in n-type Si and measured with Laplace MCTS. Both peaks are broadened as discussed in the text.

Figure 6 compares Laplace DLTS measurement of two samples; both are of hole emission at 190 K. The peak at the right of the diagram is from Mo in p-type silicon. This is a classic and well-documented defect. The only notable issue is that the peak half width is larger than that normally observed for an ideal point defect. We attribute this to bi-axial strain. The measurement was made on lightly doped epitaxial silicon deposited on a highly doped substrate.

In the case of the peak at the left of the diagram the broadening is much more substantial. The measurement was taken of hole emission from n-type material using MCTS [46] with back face illumination.

Based on the complex annealing behavior of Si:Ni Indusekhar and Kumar [47] suggested that Ni existed as a complex with a vacancy. We would expect an ideal point defect peak from such a defect and propose that the peak is due to a grouping of Ni atoms bonded in a stable configuration. The peak is reproducible but has unusual capture behavior for both holes and electrons, which will be discussed elsewhere.

3.3 Boron–oxygen Perhaps the complex, which has gained most attention in recent years is a defect associated with boron and oxygen. The efficiency of solar cells fabricated from Czochralski boron-doped silicon degrades when excess electrons are created by illumination [14]. In cells fabricated with high quality Cz material and state of the art fabrication the BO defect is now the most important non-radiative recombination route. The defect was thought to be B_sO_{2i} which from carrier lifetime spectroscopy appeared as a recombination center 0.41 eV from the conduction band with $\sigma_n/\sigma_p = 9.3$ [48, 49].

© 2012 WILEY-VCH Verlag GmbH & Co. KGaA, Weinheim

The basis for the structural assignment was a dependence of the concentration of the assumed recombination center (derived from the lifetime degradation) on $[O_i]^2$ and $[B_s]$. The formation mechanism was suggested to be the migration of the oxygen dimer to B_s via an enhanced diffusion mechanism (the dimer is normally immobile at room temperature). This enhanced diffusion was proposed as being due to a Bourgoin–Corbett mechanism under minority carrier injection [50]. This occurs in other defect systems but necessitates in this case a change in the charge state of the dimer upon capture of a minority carrier ie two charge states of the dimer must exist.

Two important studies have subsequently shown that the defect in question is unlikely to be B_sO_{2i}. Firstly, it was observed that in compensated material the degradation depended on the carrier concentration rather than the boron concentration [51]. Secondly, a study of the optical absorption spectra of the oxygen dimer showed that only one charge state exists making the Bourgoin–Corbett mechanism impossible in the case of the oxygen dimer [52].

An alternative model has been proposed by Voronkov and Falster [53] in which the defect is B_iO_{2i} formed during ingot growth. The defect is then activated by the presence of minority carriers. Several arguments have been put forward against this model including evidence that the defect density is not fixed during cooling [54] and quantitative disagreement with observations in boron compensated n-type material [55]. However in the latter case there is a question as to whether saturated concentrations of the BO complex were attained.

A crucially important dilemma is that despite many attempts no SRH defect has been observed by DLTS or related techniques, which fits the observed lifetime degradation behavior. It is evident that despite an immense amount of data and efforts by many groups throughout the world we do not as yet have a fundamental understanding of boron oxygen degradation in solar cells.

4 Recombination in multi-crystalline silicon

The situation in mc-Si is very much more complex than in single crystal material. The ingots contain grain boundaries with various degrees of mis-orientation between the grains. The material also contains dislocations and dislocation clusters within the grains. In general, mc-Si often has metallic contamination originating from the crucible material or from the use of less pure feedstock such as IMG silicon.

Neutron activation analysis has been used by several researchers to determine the level of TMs in mc-Si. Istratov et al. [56] found that the dominant metal impurities were Fe ($6 \times 10^{14}\,cm^{-3}$ to $1.5 \times 10^{16}\,cm^{-3}$), Ni (up to $1.8 \times 10^{15}\,cm^{-3}$), Co ($1.7 \times 10^{12}\,cm^{-3}$ to $9.7 \times 10^{13}\,cm^{-3}$), Mo ($6.4 \times 10^{12}\,cm^{-3}$ to $4.6 \times 10^{13}\,cm^{-3}$), and Cr ($1.7 \times 10^{12}\,cm^{-3}$ to $1.8 \times 10^{15}\,cm^{-3}$).

Macdonald et al. [57] looked at metals in different regions of cast ingots. The concentrations of Fe, Co, and Cu are determined by segregation from the liquid, which produces high concentrations near the top of the ingot, which can diffuse back into the ingot. Near the bottom, the concentrations are high due to diffusion from the crucible after crystallization has occurred. In general concentrations similar to those above were found with the addition of Cu up to $3 \times 10^{15}\,cm^{-3}$. Zn, Cr, and Si were more uniformly distributed in the ingot (2×10^{12} to $3 \times 10^{13}\,cm^{-3}$).

An experiment to examine the effect of specific metals on the electrical behavior of mc-Si was undertaken by Pizzini et al. [58]. In this work, Cz ingots were grown from intentionally contaminated feedstocks. Multicrystalline growth occurred because necking the ingot after seeding was omitted. Although the results are complicated the overall conclusion was that the presence of grain boundaries and dislocations did not enhance the detrimental effect of the metallic impurities beyond that expected for a similar metallic concentration in single crystal silicon.

Very recently, an experiment analogous to the Westinghouse study was undertaken on cast mc-Si under the EU project "CrystalClear" [59]. The project used material produced by directional solidification (Bridgeman technique) with ingots 250 mm diameter and 110 mm height. High purity feedstock and furnace components were used so without added contaminants the material had a lifetime of 60 μs. Solar cells with a p-type base of area $156\,cm^2$ were made using a classic industrial process with silicon nitride passivating/anti reflection layer, 185 μm thick with aluminium back surface field. The uncontaminated efficiency was 15.5%. The effects of Fe, Cr, Ni, Ti, and Cu on the efficiency were investigated and the Fe study has been published in considerable detail [60].

A known amount of the impurity was added to the melt and the effect on the cell efficiency determined. In the iron case the electrically active iron content was measured in the slice. In terms of the concentration of impurity added to the melt it was found that 8 ppm wt of Cr, 11 ppm wt of Fe, 0.1 ppm wt of Ti, 13 ppm wt of Ni and 8 ppm wt of Cu are all equivalents in terms of their effect on solar-cell performance giving a degradation of about 2%.

Taking into account the segregation coefficients, the rank order is the same as the Westinghouse experiment (the Cu comparison is difficult due to uncertainties regarding the effective segregation coefficient in casting processes) and the absolute concentration added to the melt for a similar degradation is of the same order. This is rather surprising when we consider that the metal distribution would be expected to be non-uniform across the slice and that far fewer atoms might be expected to be in solution due to accumulation at grain boundaries and dislocations.

On the other hand maybe this is offset by localized recombination. Sopori et al. have studied such localization in cast mc-Si, e.g. Ref. [61] and find that regions with clusters of dislocations exhibit very high recombination. In cases where the same number of dislocations are spread evenly across the cell, recombination is much reduced. This was attributed to gettering and hydrogenation being much more effective in the case of distributed dislocations. This is consistent with our work on decoration of dislocations.

 © 2012 WILEY-VCH Verlag GmbH & Co. KGaA, Weinheim

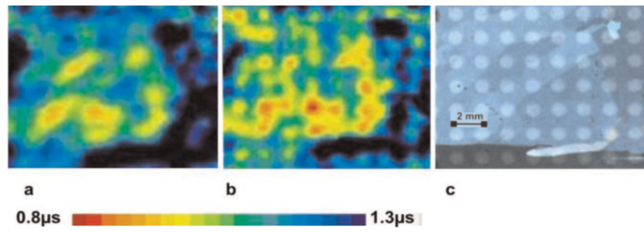

Figure 7 (online color at: www.pss-a.com) Schottky diodes on a mc-Si wafer showing (a) μPCD lifetime map on the original unpassivated slice, (b) the same region with semi-transparent diodes deposited, and (c) an optical micrograph of the diodes.

Our observation is that grain boundaries are not effective recombination centers after hydrogenation even in the presence of metals and presumably after decoration. As discussed previously in the case of large grains it is unlikely that grain boundaries will have much effect on the carrier lifetime simply because the grain size is very much larger than the diffusion length. In addition in the solar cell the minority carrier flux is parallel to the grain boundaries so will not have much effect on the photocurrent.

We have undertaken DLTS studies on solar grade mc-Si with grains in the size range 1–15 mm. The technique we have used is shown in Fig. 7 where semitransparent Schottky diodes have been deposited on mc-Si. It is possible to see the grain boundaries in the optical micrographs or by mapping the magnitude of the Raman scattering. The lifetime distribution around the diodes can also be seen.

In some slices, the DLTS signatures from diodes on grain boundaries are quite different to those relating to defects in the center of the grains. In particular, negative DLTS peaks indicating emission of minority carriers are often seen at the grain boundaries [62]. However, in many cases the DLTS spectra from different regions of the same slice show similarities. Figure 8 shows the case of a slice containing a broad distribution of dislocation clusters. The peak on the right at around 330 K was greatly reduced by hydrogenation and showed the logarithmic filling behavior of an extended defect. The family of peaks in the range 100–150 K was essentially unaffected by hydrogenation and had point defect like carrier capture. These defects have all the characteristics of powerful recombination centers.

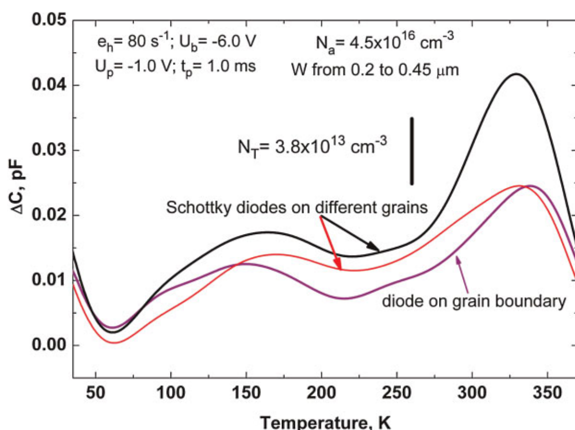

Figure 8 (online color at: www.pss-a.com) DLTS spectra of three regions of a mc-Si wafer.

5 Conclusion Our work and many cases in the literature make it evident that achieving a detailed understanding of recombination in mc-Si will be a major task. In our view, this is an essential pre-requisite to engineering effective gettering and passivation and hence to achieving very high efficiency solar cells made from these complex materials.

Acknowledgements We acknowledge funding for this work by the UK Engineering and Physical Sciences Research Council. Thanks are due to many of our colleagues for samples, advice and discussions. In particular: Bob Falster and Vladimir Voronkov (MEMC), Eike Weber (ISE), Bhushan Sopori (NREL), John Murphy (Oxford), Stefan Estreicher (Texas Tech), Alexandra Carvalho, and Jose Coutinho (Aveiro).

References

[1] J. R. Davies Jr., A. Rohatgi, R. H. Hopkins, P. D. Blais, P. Rai-Choudhury, J. R. McCormick, and H. C. Mollenkopf, IEEE Trans. Electron. Device **ED-27**, 677 (1980); A. Rohatgi, P. Rai-Choudhury, Solar Cells **17**, 119 (1986).
[2] S. Pizzini, M. Acciarri, and S. Binetti, Phys. Status Solidi A **202**, 2928 (2005).
[3] A. A. Istratov and E. R. Weber, Appl. Phys. A **66**, 123 (1998).
[4] T. Buonassisi, A. A. Istratov, M. D. Pickett, M. Heuer, J. P. Kalejs, G. Hahn, M. A. Marcus, B. Lai, Z. Cai, S. M. Heald, T. F. Ciszek, R. F. Clark, D. W. Cunningham, A. M. Gabor, R. Jonczyk, S. Narayanan, E. Sauar, and E. R. Weber, Prog. Photovolt. Res. Appl. **14**, 513 (2006).
[5] S. Hocine and D. Mathiot, Appl. Phys. Lett. **53**, 1269 (1988).
[6] T. Sadoh and H. Nakashima, Appl. Phys. Lett. **58**, 1653 (1991).
[7] E. R. Weber, Appl. Phys. A **30**, 1 (1983).
[8] E. Weber and H. G. Riotte, J. Appl. Phys. **51**, 1484 (1980).
[9] J. D. Struthers, J. Appl. Phys. **27**, 1560 (1956).
[10] H. Kitagawa and K. Hashimoto, Jpn. J. Appl. Phys. **16**, 857 (1977); H. Kitagawa, and K. Hashimoto, Jpn. J. Appl. Phys. **16**, 173 (1977).
[11] A. A. Istratov, P. Zhang, R. J. McDonald, A. R. Smith, M. Seacrist, J. Moreland, J. Shen, R. Wahlich, and E. R. Weber, J. Appl. Phys. **97**, 023505 (2005).
[12] R. N. Hall and J. H. Racette, J. Appl. Phys. **35**, 379 (1964).
[13] J. L. Benton, D. C. Jacobson, B. Jackson, J. A. Johnson, T. Boone, D. J. Eaglesham, F. A. Stevie, and J. Becerro, J. Electrochem. Soc. **146**, (1929). (1999.
[14] J. Schmidt and A. Cuevas, J. Appl. Phys. **86**, 3175 (1999).
[15] J. Schmidt, R. Krain, K. Bothe, G. Pensl, and S. Beljakowa, J. Appl. Phys. **102**, 123701 (2007); S. Diez, S. Rein, T. Roth, and S. W. Glunz, J. Appl. Phys. **101**, 033710 (2007).
[16] S. Rein, T. Rehrl, W. Warta, and S. W. Glunz, J. Appl. Phys. **91**, 2059 (2002).
[17] D. K. Schroder, Semiconductor Material and Device Characterization (John Wiley, Hoboken, 2006), chap. 7.
[18] A. C. Wang and C. T. Sah, J. Appl. Phys. **56**, 1021 (1984).
[19] T. Sadoh, H. Nakashima, and T. Tsurushima, J. Appl. Phys. **72**, 520 (1992).

© 2012 WILEY-VCH Verlag GmbH & Co. KGaA, Weinheim

[20] H. Conzelmann, K. Graff, and E. R. Weber, Appl. Phys. A **30**, 169 (1983).
[21] T. Roth, P. Rosenits, S. Diez, S. W. Glunz, D. Macdonald, S. Beljakowa, and G. Pensl, J. Appl. Phys. **102**, 103716 (2007).
[22] A. A. Istratov, H. Hieslmair, and E. R. Weber, Appl. Phys. A **69**, 13 (1999).
[23] R. H. Wu and A. R. Peaker, Solid Stat Electron. **25**, 643 (1982).
[24] P. Deixler, J. Terry, I. D. Hawkins, J. H. Evans-Freeman, A. R. Peaker, A. L. Rubaldo, D. K. Maude, J.-C. Portal, K. Bonde Nielsen, A. Nylandsted Larsen, and A. Mesli, Appl. Phys. Lett. **73**, 3126 (1998).
[25] L. Rubaldo, P. Deixler, I. D. Hawkins, J. Terry, D. K. Maude, J.-C. Portal, J. H. Evans-Freeman, L. Dobaczewski, and A. R. Peaker, Mater. Sci. Eng. B **58**, 126 (1999).
[26] H. Lemke, Phys. Status Solidi A **64**, 215 (1981).
[27] G. Zoth and W. Bergholz, J. Appl. Phys. **67**, 6764 (1990).
[28] A. R. Peaker, V. P. Markevich, and L. Dobaczewski, Hydrogen-Related Defects in Silicon, Germanium, and Silicon–Germanium Alloys, in: Defects in Microelectronic Materials and Devices, edited by D. M. Fleetwood, S. T. Pantelides, and R. D. Schrimpf, (eds.), (CRC Press, Boca Raton, 2009). chap. 2.
[29] L. Dobaczewski, A. R. Peaker, and K. Bonde Nielsen, J. Appl. Phys. **96**, 4689 (2004). www.laplacedlts.eu.
[30] D. West, S. K. Estreicher, S. Knack, and J. Weber, Phys. Rev. B **68**, 035210 (2003).
[31] W. Jost and J. Weber, Phys. Rev. B **54**, R11038 (1996).
[32] D. J. Backlund and S. K. Estreicher, Phys. Rev. B **81**, 235213 (2010).
[33] M. Shiraishi, J.-U. Sachse, H. Lemke, and J. Weber, Mater. Sci. Eng. B **58**, 130 (1999).
[34] S. Knack, J. Weber, H. Lemke, and H. Riemann, Phys. Rev. B **65**, 165203 (2002).
[35] D. West and S. K. Estreicher, Phys. Rev. B **68**, 035210 (2003).
[36] C. D. Latham, M. Alatalo, R. M. Nieminen, R. Jones, S. Öberg, and P. R. Briddon, Phys. Rev. B **72**, 235205 (2005).
[37] G. Sarau, A. Bochmann, S. Christiansen, and S. Schönfelder, 35th Photovoltaic Specialists Conference (PVSC), Honolulu, USA, 2010 IEEE, pp. 699–6703; G. Sarau, S. Christiansen, R. Lewandowska, and B. Roussel, 35th Photovoltaic Specialists Conference (PVSC), Honolulu, USA, 2010 IEEE, pp. 1770–1775.
[38] P. Omling, E. R. Weber, L. Montelius, H. Alexander, and J. Michel, Phys. Rev. B **32**, 6571 (1985).
[39] J. Kaniewski, M. Kaniewska, and A. R. Peaker, Appl. Phys. Lett. **60**, 359 (1992).
[40] M. Saritas and A. R. Peaker, Solid State Electron. **38**, 1025 (1995).
[41] A. Berg, I. Brough, J. H. Evans, G. Lorimer, and A. R. Peaker, Semicond. Sci. Technol. **7**, A263 (1992).
[42] V. Kveder, M. Kittler, and W. Schröter, Phys. Rev. B **63**, 115208 (2001).
[43] X. Yu, X. Li, R. Fan, D. Yang, M. Kittler, M. Reiche, M. Seibt, and G. Rozgonyi, J. Appl. Phys. **108**, 053719 (2010).
[44] M. Steger, A. Yang, T. Sekiguchi, K. Saeedi, M. L. W. Thewalt, M. O. Henry, K. Johnston, H. Riemann, N. V. Abrosimov, M. F. Churbanov, A. V. Gusev, A. K. Kaliteevskii, O. N. Godisov, P. Becker, and H.-J. Pohl, J. Appl. Phys. **110**, 081301 (2011).
[45] A. Carvalho, D. J. Backlund, and S. K. Estreicher, Phys. Rev. B **84**, 155322 (2011).
[46] R. Brunwin, B. Hamilton, P. Jordan, and A. R. Peaker, Electron Lett. **15**, 349–3350 (1979).
[47] H. Indusekhar and V. Kumar, J. Appl. Phys. **61**, 1449 (1987).
[48] S. Rein and S. W. Glunz, Appl. Phys. Lett. **82**, 1054 (2003).
[49] K. Bothe and J. Schmidt, J. Appl. Phys. **99**, 013701 (2006).
[50] J. Adey, R. Jones, D. W. Palmer, P. R. Briddon, and S. Öberg, Phys. Rev. Lett. **93**, 055504 (2004).
[51] D. Macdonald, F. Rougieux, A. Cuevas, B. Lim, J. Schmidt, M. Di Sabatino, and L. J. Geerligs, J. Appl. Phys. **105**, 093704 (2009).
[52] L. I. Murin, E. A. Tolkacheva, V. P. Markevich, A. R. Peaker, B. Hamilton, E. Monakhov, B. G. Svensson, J. L. Lindström, P. Santos, J. Coutinho, and A. Carvalho, Appl. Phys. Lett. **98**, 182101 (2011).
[53] V. V. Voronkov and R. Falster, J. Appl. Phys. **107**, 053509 (2010).
[54] F. E. Rougieux, B. Lim, J. Schmidt, M. Forster, D. Macdonald, and A. Cuevas, J. Appl. Phys. **110**, 063708 (2011).
[55] D. Macdonald, A. Liu, A. Cuevas, B. Lim, and J. Schmidt, Phys. Status Solidi A **208**, 559 (2011).
[56] A. A. Istratov, T. Buonassisi, R. J. McDonald, A. R. Smith, R. Schindler, J. A. Rand, J. P. Kalejs, and E. R. Weber, J. Appl. Phys. **94**, 6552–6559 (2003).
[57] D. Macdonald, A. Cuevas, A. Kinomura, Y. Nakano, and L. J. Geerligs, J. Appl. Phys. **97**, 033523 (2005).
[58] S. Pizzini, L. Bigoni, and M. Beghi, J. Electrochem. Soc. **133**, 2363 (1986).
[59] G. Coletti, P. C. P. Bronsveld, G. Hahn, W. Warta, D. Macdonald, B. Ceccaroli, K. Wambach, N. Le Quang, and J. M. Fernandez, Adv. Funct. Mater. **21**, 879 (2011).
[60] G. Coletti, R. Kvande, V. D. Mihailetchi, L. J. Geerligs, L. Arnberg, and E. J. Øvrelid, J. Appl. Phys. **104**, 104913 (2008).
[61] B. Sopori, P. Rupnowski, S. Shet, V. Budhraja, N. Call, S. Johnston, M. Seacrist, G. Shi, J. Chen, and A. Deshpande, 35th Photovoltaic Specialists Conference (PVSC), Honolulu, USA, 2010 IEEE, pp. 2233–2237.
[62] Y. Liya, PhD Thesis 2011, Dept. of Materials Science and Engineering, North Carolina State University, Raleigh, 27606, USA.

 © 2012 WILEY-VCH Verlag GmbH & Co. KGaA, Weinheim